Available online at ScienceDirect

Nuclear Engineering and Technology

journal homepage: www.elsevier.com/locate/net

Original Article

Study of the Changes in Composition of Ammonium Diuranate with Progress of Precipitation, and Study of the Properties of Ammonium Diuranate and its Subsequent Products Produced from both Uranyl Nitrate and Uranyl Fluoride Solutions

Subhankar Manna [a,b,*], *Raj Kumar* [a], *Santosh K. Satpati* [a], *Saswati B. Roy* [a], *and Jyeshtharaj B. Joshi* [b,c]

[a] *Bhabha Atomic Research Centre, Trombay, Mumbai 400 085, India*
[b] *Homi Bhabha National Institute (HBNI), Anushakti Nagar, Mumbai 400 094, India*
[c] *Department of Chemical Engineering, Institute of Chemical Technology, Nathalal Parekh Marg, Matunga, Mumbai 400 019, India*

ARTICLE INFO

Article history:
Received 18 July 2016
Received in revised form
20 September 2016
Accepted 21 September 2016
Available online 14 October 2016

Keywords:
Ammonium diuranate
Crystal structure
UF4
UO2
UO3

ABSTRACT

Uranium metal used for fabrication of fuel for research reactors in India is generally produced by magnesio-thermic reduction of UF_4. Performance of magnesio-thermic reaction and recovery and quality of uranium largely depends on properties of UF_4. As ammonium diuranate (ADU) is first product in powder form in the process flow-sheet, properties of UF_4 depend on properties of ADU. ADU is generally produced from uranyl nitrate solution (UNS) for natural uranium metal production and from uranyl fluoride solution (UFS) for low enriched uranium metal production. In present paper, ADU has been produced via both the routes. Variation of uranium recovery and crystal structure and composition of ADU with progress in precipitation reaction has been studied with special attention on first appearance of the precipitate Further, ADU produced by two routes have been calcined to UO_3, then reduced to UO_2 and hydroflorinated to UF_4. Effect of two different process routes of ADU precipitation on the characteristics of ADU, UO_3, UO_2 and UF_4 were studied here.

* *Corresponding author.*
E-mail addresses: smanna@barc.gov.in, subhankarmanna@yahoo.co.in (S. Manna).
http://dx.doi.org/10.1016/j.net.2016.09.005

1. Introduction

The role of research reactors for the development of a nuclear program of any country is well established [1–3]. Research reactors are utilized to produce radioisotopes and offer irradiation facilities for testing various nuclear fuel and structural materials [4,5]. Radioisotopes such as Co-60, Cs-137, and I-131 are used in the fields of medicine, industries, agriculture, and food processing [6]. Apart from these, research reactors are also used for neutron beam research activity, testing neutron detectors, testing materials for mew power plant, training of manpower, etc. With a rapid expansion of the nuclear program in India, more research reactors are needed for nuclear technology as they contribute to the creation of essential infrastructure for research and for building capabilities. Metallic uranium of very high purity has been used for the production of research reactor fuel. Uranium production processes are categorized into four groups as follows: (1) reduction of uranium halides with metals, (2) reduction of uranium oxides with metal and carbon, (3) electrolytic reduction, and (4) disproportionation or thermal decomposition of uranium halides [7]. Reduction of uranium tetrafluoride with calcium or magnesium is one of the main industrial methods for producing pure uranium ingot. Ammonium diuranate (ADU) is the first intermediate product in solid powder form in the flow sheet of uranium metal ingot production [8]. ADU is generally produced from uranyl nitrate for natural uranium fuel production and from uranyl fluoride for low enriched uranium fuel production. In both the production processes, uranyl solution (either nitrate or fluoride) reacts with ammonia (either gaseous or aqueous form) and precipitation occurs when the concentration of the product (ADU) exceeds its solubility.

$$UO_2(NO_3)_2 + NH_3 + H_2O \rightarrow (NH_4)_2U_2O_7\ (ADU) \downarrow + NH_4NO_3 + H_2O \quad (1)$$

$$UO_2F_2 + NH_3 + H_2O \rightarrow (NH_4)_2U_2O_7\ (ADU) \downarrow + NH_4F + H_2O \quad (2)$$

This process is called reactive precipitation or crystallization. Reaction, nucleation, growth, agglomeration, and breakage are the kinetics of reactive precipitation [9,10]. As the formula suggests, the ratio of NH_3:U should be 1; however, several authors [11–18] reported variable NH_3:U ratios, varying from 0.15 to 0.6 depending on the production procedure. However, practically no systematic study was carried out to observe how the composition and structure of ammonium uranate change during the course of precipitation. ADU is further calcined to UO_3. The UO_3 is then reduced to UO_2, followed by hydrofluorination of UO_2 to UF_4. Uranium metal ingot is produced by magnesio-thermic reduction (MTR) of UF_4. The performance of MTR reaction and recovery of uranium largely depend on the properties of UF_4 [19–21]. UF_4 normally contains a small amount of uranyl fluoride (UO_2F_2), known as a water-soluble content; unconverted uranium oxides; moisture, and a small amount of free acid (HF). UO_2F_2 in UF_4 plays a major role in the reduction reaction. UO_2F_2, when heated in the presence of moisture, hydrolyzes to UO_3 and HF. UO_3 remains unreduced during the MTR, and as a result, the bomb yield decreases. HF reacts with magnesium and forms a refractory MgF_2 film on magnesium, which hinders the vaporization of magnesium chips and the triggering of the reaction is delayed. Hydrogen generated by this side reaction reacts with UO_2F_2, producing harmful HF again. The unconverted uranium oxide present in the green salt is a mixture of all the unhydrofluorinated oxides. These oxides neither get reduced during the course of the reaction nor get dissolved in the slag, and as a result, reduce the fluidity of the slag and the separation of metal and slag. The tap density of UF_4 is also important for the performance of MTR operation [5,21]. In the present study, ADU has been produced by reactions of gaseous ammonia with both uranyl nitrate and uranyl fluoride. The progress of ADU precipitation has been observed very closely, with special attention on the first appearance of the precipitate for both nitrate and fluoride routes. Changes of recovery and composition with pH and time have also been observed during the course of precipitation. ADU produced by both the routes have been calcined to UO_3, further reduced to UO_2, and hydrofluorinated to UF_4 under similar conditions. Both chemical and physical properties of the products have been analyzed carefully to understand how the properties of UF_4 are inherited from its precursors.

2. Materials and methods

ADU precipitation reaction was carried out in a 3 L agitated glass reactor (10 of Fig. 1) of 0.150 m diameter. The reactor was fitted with four equally spaced 15-mm-wide baffles. A

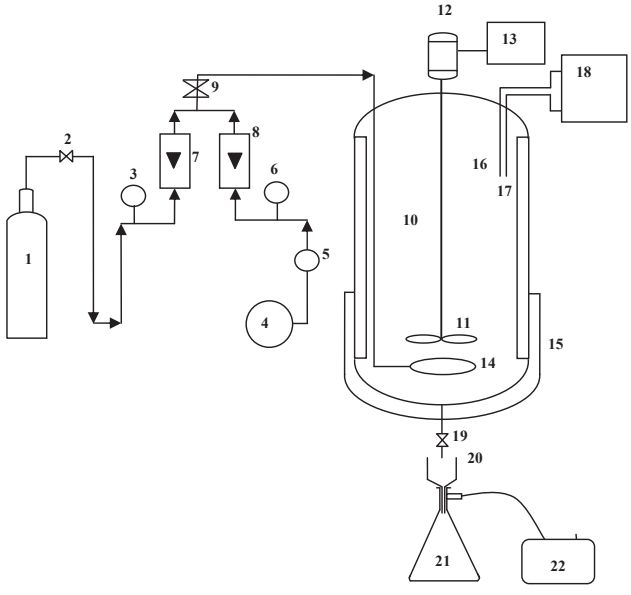

Fig. 1 – Schematic diagram of ADU precipitation system. The numbers in the figure represent the following: 1, ammonia gas cylinder; 2, pressure reducing valve; 3, pressure gauge; 4, air compressor; 5, pressure regulator; 6, pressure gauge; 7, NH_3 rotameter; 8, air rotameter; 9, nonreturn valve; 10, glass reactor; 11, impeller; 12, motor; 13, variable frequency drive; 14, sparger; 15, muffle heater; 16, pH electrode; 17, PT 100 RTD; 18, pH meter; 19, bottom valve; 20, Buchner funnel; 21, conical flask; and 22, vacuum pump.

schematic drawing of the precipitator is shown in Fig. 1. Gaseous ammonia (99.9% pure) from a commercial-grade ammonia cylinder (1) was mixed with air from a compressor (4) at a ratio of 1:10, and the mixture gas was introduced through a ring sparger (14). The flow rates of ammonia and air were continuously controlled using two separate valves and calibrated rotameters (7 and 8). Uranium concentration and temperature of both the feed solutions were 65 g/L and 50°C, respectively. A pitched blade turbine-type impeller (11) was used, and the rotational speed of the impeller was maintained at 8.33 r/s. To study the progress of the ADU precipitation process, pH of the solution was continuously monitored through a pH meter (18). Samples (aliquot) were withdrawn after regular intervals. The collected samples were filtered using a Büchner funnel (20) connected with a vacuum pump (22), and the filtrate was collected in a conical flask (21). The cake was then washed with distilled water. The pH and uranium concentration in the filtrate were measured. Furthermore, the cake was naturally dried. The crystal structure of dried ADU was measured using X-ray diffraction or XRD (Model: Equinox 3000; INEL) with a position sensitive detector (PSD) detector at 40 kV and 30 mA with Cu Kα (1.5406 Å) radiation. Furthermore, the final ADU, produced from both uranyl nitrate solution (UNS) and uranyl fluoride solution (UFS), was calcined in similar condition. Calcination was carried out in a box-type furnace (Fig. 2). Temperature was increased from room temperature to 550°C at a ramp rate of 5°C/min and then maintained at 550°C for 4 hours. Then the heating was stopped. The crystal structure, fluoride content, particle size, specific surface area (SSA), and O/U ratio of UO_3 were measured. Furthermore, UO_3 was reduced by passing NH_3 gas over the static bed of UO_3 at 750°C inside a box furnace (Fig. 3). The furnace was heated at a ramp rate of 6.25°C/min, and argon was fed continuously until the temperature reached 750°C. NH_3 gas was then fed over UO_3 at a rate of 8–10 L/min. Similar operating conditions were maintained in both cases. The crystal structure, fluoride content, particle size, SSA, and O/U ratio of UO_2 were measured. UF_4 was produced thereafter by passing anhydrous HF gas over the static bed of UO_2 at 450°C inside a box furnace. A schematic drawing of the hydrofluorination furnace is shown in Fig. 4. The furnace was heated at a ramp rate of 5°C/min. Argon was purged until the temperature reached 450°C. HF was then purged for 30 minutes at 450°C. Similar operating conditions were maintained in both cases. The crystal structure, particle size, tap density, and UO_2F_2 and

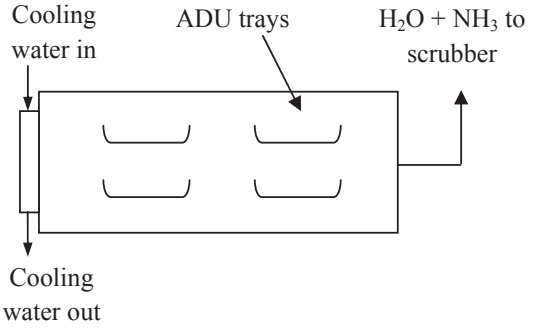

Fig. 2 – Schematic diagram of ADU calcination system. ADU, ammonium diuranate.

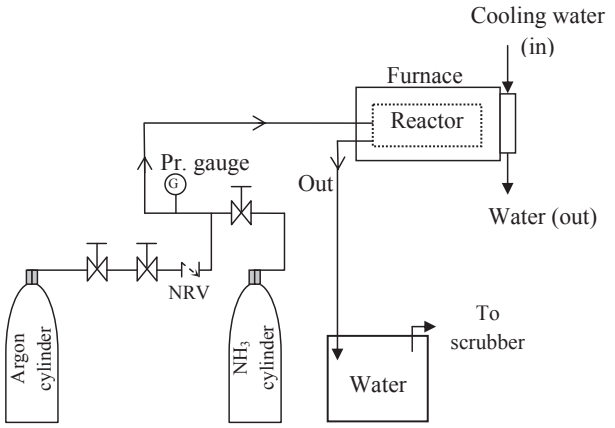

Fig. 3 – Schematic diagram of UO_3 reduction system. NRV, non return valve; Pr., pressure.

uranium oxide contents of UF_4 were measured. A list of the instruments and methodologies used is shown in Table 1.

3. Results and discussion

In the present study, ADU was produced by two different routes: (1) by reaction of UNS with gaseous ammonia (ADUI) and (2) by reaction of UFS with gaseous ammonia (ADUII). Studies on the progress of ADU precipitation in both routes were carried out, with special attention on the first appearance of the precipitate and changes in uranium recovery and crystal structure with time. Then ADU produced by the two routes were calcined to UO_3, further reduced to UO_2, and hydrofluorinated to UF_4. The effect of the two different process routes of ADU precipitation on the characteristics of ADU, UO_3, UO_2, and UF_4 were studied here.

3.1. *Changes in pH, uranium recovery, and structure of ADU with progress of precipitation reaction*

Variation in pH and uranium recovery in filtrate with time, during ADU precipitation from UNS, is shown in Fig. 5. It was

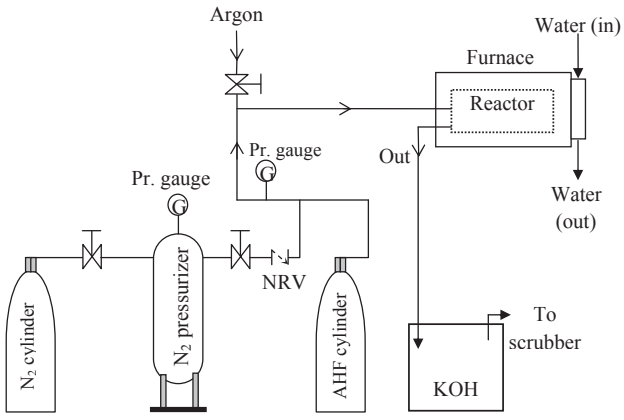

Fig. 4 – Schematic diagram of UO_2 hydrofluorination system. AHF, anhydrous hydrogen fluoride; NRV, non return valve; Pr., pressure.

Table 1 – List of instruments/methodologies.

Sr. No.	Properties	Method/instrument used
1	pH	pH meter: 10 PHM 11
2	Uranium	Volumetry ICPAES: ASX-520 autosampler
3	XRD	Powder diffractometer: INEL Equinox 3000
4	% Fluoride	Ion selective electrode: Orion 700+
5	Particle size analysis	Laser particle size analyzer: CILAS 1180
6	Specific surface area	Brunner–Emmet–Teller: SURFER
7	Tap density	Tapping as per ASTM B-527, 1976
8	O/U ratio	Gravimetry
9	UO_2F_2	Spectrophotometry: UNICAM-UV
10	Unconverted uranium oxide	Gravimetry

XRD, X-ray diffraction; ICPAES, inductively coupled plasma atomic emission spectroscopy.

observed that initially there was a slow increase of pH (region 0–1), then there was a sudden small reduction in pH (region 1–2) followed by an almost flat zone (region 2–3), and then there was a sharp increase in pH (region 3–4) followed by a slow increase in pH (region 4–5). The explanation for this is that initially ammonia neutralized the free acid present in the UNS; as a result, pH of the solution was increased. A small reduction of pH occurred due to the generation of H^+ ions at the start of precipitation [22]. It was further noticed from the uranium recovery versus time plot that precipitation started only after reaching a certain pH. Recovery has been calculated based on the initial concentration of uranium in the solution and the concentration of uranium in the filtrate at any moment. The first precipitation point was detected by the appearance of permanent turbidity, which was found to coincide with the reduction of pH. It was also observed that around 90% recovery of uranium took place at the end of the flat zone. Recovery was further increased to 99.98% when pH reached 7.5. Almost no improvement in recovery was observed when pH was further increased to 8.5. Slurry samples were collected at the first precipitation point (I1; pH 3.19), in between (I2; pH 3.18) the flat zone, at the end point (I3; pH 3.52) of the flat zone, at pH 7.5 (I4), and at pH 8.5 (I5). ADUI1 was very sticky and became hard lumps during drying. ADUI2 and ADUI3 were not sticky, but they became soft lumps during drying. ADUI4 and ADUI5 were very easily filterable and converted to powder during drying. XRD patterns of these ADUs are shown in Fig. 6. The color of the ADU at every stage of the reaction was yellowish. ADUI1 and ADUI2 were found to be orthorhombic $3UO_3.NH_3.5H_2O$ (JCPDF 043-0365) [16]. It was also noticed that another phase appeared with a further increase of ammonia addition. It was studied that ADUI3, ADUI4, and ADUI5 were multiphasic compounds, and consisted of orthorhombic $3UO_3.NH_3.5H_2O$ and hexagonal $2UO_3.NH_3.3H_2O$ (JCPDF 044-0069) [16]. It was further observed that with an increase of ammonia addition, dominancy of the hexagonal structure was increased.

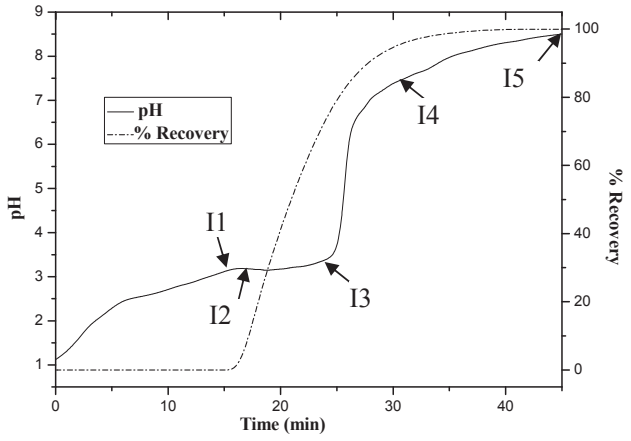

Fig. 5 – Changes in pH and % uranium recovery with time during ADU precipitation by reaction of UNS with gaseous ammonia. ADU, ammonium diuranate; UNS, uranyl nitrate solution.

Variation of pH and uranium concentration with time during ADU precipitation by the reaction between UFS and gaseous ammonium is shown in Fig. 7. Unlike Fig. 5, pH of the solution was increased continuously and no flat zone was observed in the graph. However, precipitation started only after reaching a certain pH as earlier, but the pH (at pH 5.98) was higher than that in case of precipitation from UNS (at pH 3.19). Recovery of uranium at any pH in the UFS route was lower than that in the UNS route. More than 99% recovery was observed only at and above pH 9. Total time required for 99% conversion was 143 minutes from UFS, whereas it was only 32 minutes from UNS.

Slurry samples were collected at the first precipitation point (II1; pH 5.98), pH 6.74 (II2), pH 7.5 (II3), pH 7.85 (II4), pH 8.5 (II5), and pH 9 (II6). Green gelatinous precipitate (ADUII1) was obtained at the inception. ADUII2 and ADUII3 were little sticky and became hard lumps during drying. ADUII4 was not sticky and became soft lumps during drying. ADUII5 and ADUII6 were easily filterable and became powder on pressing during

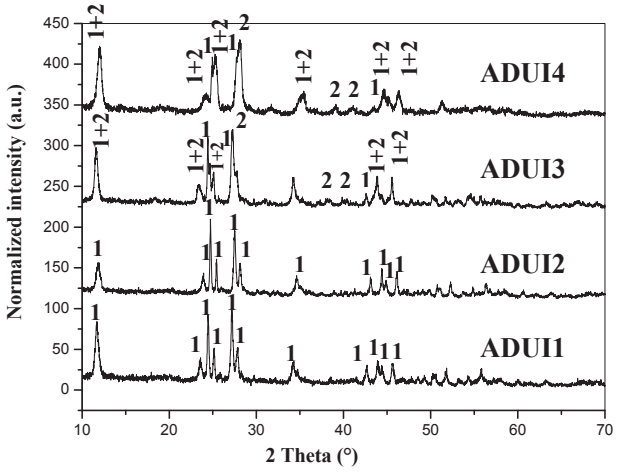

Fig. 6 – XRD images of ADU produced at different times during ADU precipitation by reaction of UNS with gaseous ammonia. The numbers in the figure represent the following: 1, $3UO_3.NH_3.5H_2O$, orthorhombic; and 2, $2UO_3.NH_3.3H_2O$, hexagonal. ADU, ammonium diuranate; UNS, uranyl nitrate solution; XRD, X-ray diffraction.

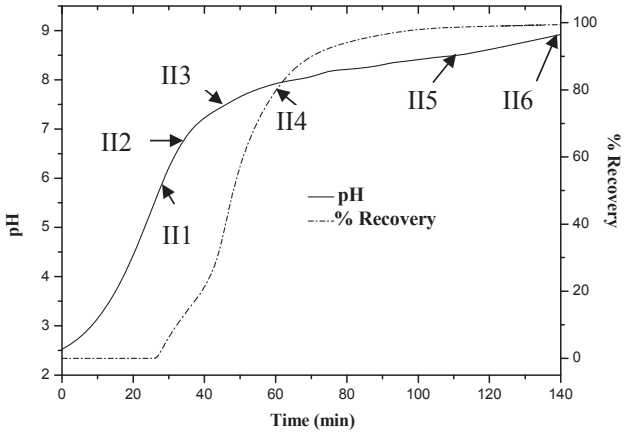

Fig. 7 – Changes in pH and uranium concentration with time during ADU precipitation by reaction of UNS with gaseous ammonia. ADU, ammonium diuranate; UNS, uranyl nitrate solution.

drying. The color of the ADU was nicely changed from green to khaki to brownish to greenish yellow. An XRD pattern of these ADUs is shown in Fig. 8. It has been observed that ADU produced at the inception (ADUII1) consisted of orthorhombic $(NH_4)_3UO_2F_5$ (JCPDF 021-0802) [23]. ADUII2 consisted of orthorhombic $(NH_4)_3UO_2F_5$ and $(NH_4)(UO_2)_2F_5.4H_2O$ (hexagonal) (JCPDF 026-0095) [24], with dominancy of $(NH_4)_3UO_2F_5$. ADUII3 consisted of $(NH_4)_3UO_2F_5$, $(NH_4)(UO_2)_2F_5.4H_2O$, and hexagonal $2UO_3.NH_3.3H_2O$ (JCPDF 044-0069) [16], with dominancy of $(NH_4)_3UO_2F_5$. ADUII4–ADUII6 consisted of $(NH_4)_3UO_2F_5$), $(NH_4)(UO_2)_2F_5.4H_2O$, and $2UO_3.NH_3.3H_2O$, with increased dominancy of $2UO_3.NH_3.3H_2O$, which increased with ammonia addition.

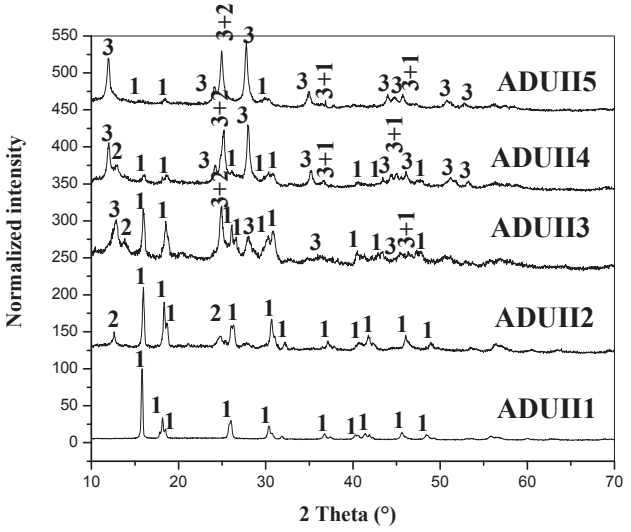

Fig. 8 – XRD images of ADU produced at different times during ADU precipitation by reaction of UFS with gaseous ammonia. The numbers in the figure represent the following: 1, $(NH_4)_3UO_2F_5$, orthorhombic; 2, $(NH_4).(UO_2)_2F_5.4H_2O$, hexagonal; and 3, $2UO_3.NH_3.3H_2O$, hexagonal. ADU, ammonium diuranate; UFS, uranyl fluoride solution; XRD, X-ray diffraction.

3.2. *Effect of two different process routes of ADU precipitation on the characteristics of ADU, UO_3, UO_2, and UF_4*

The final ADU, which was produced via UNS (ADUI4) and UFS (ADUII6) routes, was further calcined, reduced, and then hydrofluorinated under similar conditions. UO_3, UO_2, and UF_4, which were produced via the UNS route, are written as UO_3I, UO_2I, and UF_4I, respectively, and UO_3, UO_2, and UF_4, which were produced via the UFS route, are written as UO_3II, UO_2II, and UF_4II, respectively. It has been observed from Table 2 that UO_2F_2 and uranium oxide contents were more in UF_4 obtained via the UFS route than in that obtained via the UNS route. UO_2F_2 has been generated due to the reaction of HF with unconverted UO_3 present in UO_2, which depends on the conversion of UO_3 to UO_2 and indicated by the O/U ratio of UO_2. The more the O/U ratio of UO_2, the more the presence of UO_3 in UO_2. Conversion of UO_3 to UO_2 depends on an SSA of UO_3 and the O/U ratio of UO_3. Table 3 indicates that the SSA of UO_3 obtained from the UNS route is more than that obtained from the UFS route. The SSA of UO_3 mainly depends on the particle size and morphology of UO_3. It has been noted from Table 3 that the mean particle size of UO_3 obtained from the UFS route is more than that of the UNS route. Ammonia released during calcination reduces UO_3 [25,26]. Reduction of calcined product of ADU produced via the UFS route is less due to the presence of fluoride in ADU. As a result, the O/U ratio of UO_3 from the UNS route is lesser than that from the UFS route. The content of uranium oxide in UF_4 indicates conversion of UO_2 to UF_4, which depends on the SSA of UO_2. Table 4 shows that the SSA of UO_2 obtained from the UNS route is more than that from the UFS route. Similarly, the SSA of UO_2 mainly depends on the particle size and morphology of UO_2. It has been observed from Table 4 that the mean particle size of UO_2 obtained from the UFS route is more than that from the UNS route. It is further noticed that the tap density of UF_4 obtained from the UNS route is more than that from the UFS route (Table 2). It has been observed from Table

Table 2 – Physical and chemical properties of UF_4.

Sr. No.	UF_4 sample No.	UO_2F_2 (weight %)	Unconverted uranium oxide (weight%)	Mean particle size (μm)	TD (g/cc)
1	UF_4I	0.64	0.17	17.53	2.45
2	UF_4II	1.13	0.52	22.75	2.37

TD, tap density.

Table 3 – Physical and chemical properties of UO_3.

Sr. No.	UO_3 sample No.	Fluoride (weight%)	O/U ratio	Mean particle size (μm)	SSA (m^2/g)	TD (g/cc)
1	UO_3I	–	2.70	19	27.59	2.31
2	UO_3II	0.15	2.79	23.28	21.03	2.19

SSA, specific surface area; TD, tap density.

Table 4 – Physical and chemical properties of UO_2.

Sr. No.	UO_2 sample No.	Fluoride (weight%)	O/U ratio	Mean particle size (μm)	SSA (m^2/g)	TD (g/cc)
1	UO_2I		2.06	16.34	19.21	2.53
2	UO_2II	0.0323	2.09	21.03	15.36	2.41

SSA, specific surface area; TD, tap density.

Table 5 – Physical and chemical properties of ADU.

Sr. no.	ADU sample No.	Fluoride (weight %)	Mean particle size (μm)	SSA (m^2/g)	TD (g/cc)
1	ADUI	–	19.91	20.93	2.26
2	ADUII	2.21	23.88	17.72	2.18

ADU, ammonium diuranate; SSA, specific surface area; TD, tap density.

5 that the mean particle size of ADU obtained from the UFS route is more than that from the UNS route, and the SSA of ADU obtained from the UNS route is more than that from the UFS route. It is further noted that particle size was reduced from ADU to UO_3 to UO_2 to UF_4.

The XRD pattern (Fig. 9) shows that ADUI4 consisted of orthorhombic $3UO_3.NH_3.5H_2O$ (PDF 043-0365) and hexagonal $2UO_3.NH_3.3H_2O$ (PDF 044-0069), and ADUII6 consisted of orthorhombic $(NH_4)_3UO_2F_5$ (JCPDF 021-0802), hexagonal $(NH_4).(UO_2)_2F_5.4H_2O$ (PDF 026-0095), and hexagonal $2UO_3.NH_3.3H_2O$, with dominancy of $2UO_3.NH_3.3H_2O$. The XRD patterns of the calcined product of ADU, produced from both

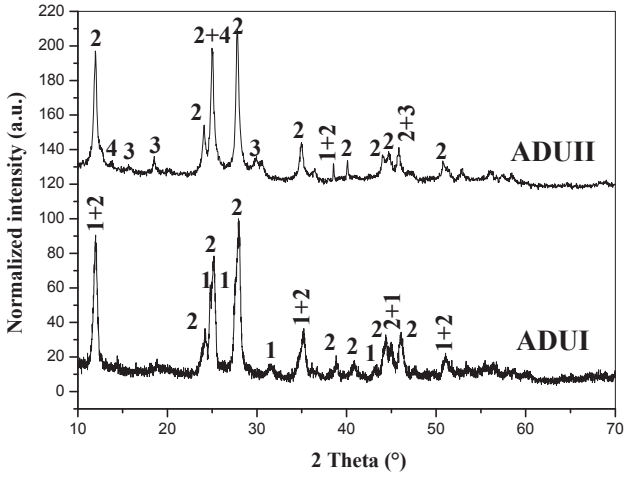

Fig. 9 – XRD patterns of ADU produced from UNS and UFS. The numbers in the figure represent the following: 1, $3UO_3.NH_3.5H_2O$, orthorhombic; 2, $2UO_3.NH_3.3H_2O$, hexagonal; 3, $(NH_4)_3UO_2F_5$, orthorhombic; and 4, $(NH_4).(UO_2)_2F_5.4H_2O$, hexagonal. ADU, ammonium diuranate; UFS, uranyl fluoride solution; UNS, uranyl nitrate solution; XRD, X-ray diffraction.

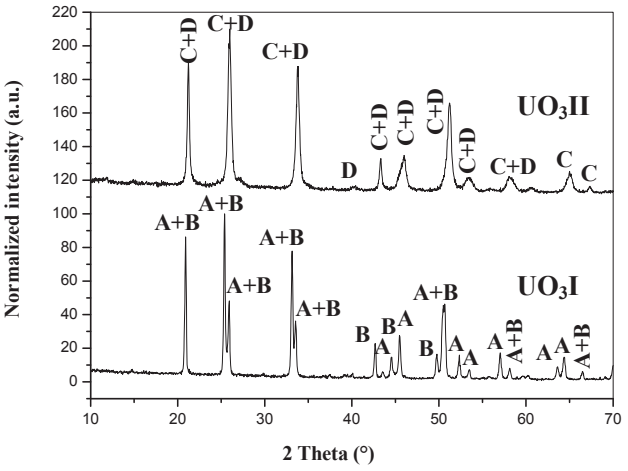

Fig. 10 – XRD patterns of UO_3 produced via UNS and UFS routes. In the figure, letter A represents orthorhombic UO_3, B represents orthorhombic U_3O_8, C represents hexagonal UO_3, and D represents hexagonal U_3O_8. ADU, ammonium diuranate; UFS, uranyl fluoride solution; UNS, uranyl nitrate solution; XRD, X-ray diffraction.

UNS and UFS routes, are shown in Fig. 10. Both the UO_3I and the UO_3II are basically mixture of UO_3 and U_3O_8, which is clearly indicated by O/U ratio of UO_3 (Table 3). It is further observed from the XRD patterns that UO_3I consisted of orthorhombic UO_3 (PDF 072-0246) [27] and orthorhombic U_3O_8 (PDF 047-1493) [28], and UO_3II consisted of hexagonal UO_3 (PDF 031-1416) [29] and hexagonal U_3O_8 (PDF 074-2102) [30]. However, both patterns (Fig. 11) of UO_2 matched with those reported in the International Centre for Diffraction Data (ICDD) database (PDF number 00-041-1422) [31] for the cubic structure. X-ray phase analysis (Fig. 12) of UF_4I and UF_4II matched with those reported in the ICDD database (PDF number 082-2317) [32] for the monoclinic structure.

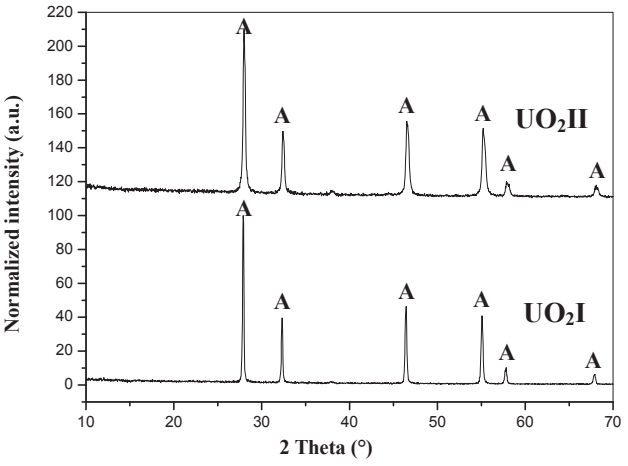

Fig. 11 – XRD patterns of UO_2 produced via UNS and UFS routes. In the figure, letter A represents cubic UO_2. ADU, ammonium diuranate; UFS, uranyl fluoride solution; UNS, uranyl nitrate solution; XRD, X-ray diffraction.

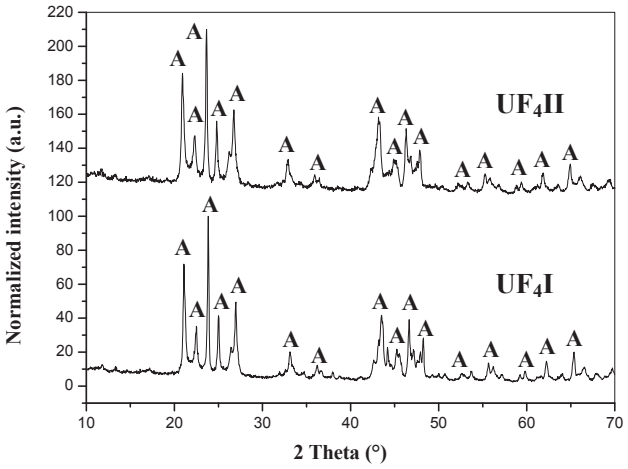

Fig. 12 – XRD patterns of UF_4 produced via UNS and UFS routes. In the figure, letter A represents monoclinic UF_4. ADU, ammonium diuranate; UFS, uranyl fluoride solution; UNS, uranyl nitrate solution; XRD, X-ray diffraction.

4. Conclusion

Uranium metal used for fabrication of fuel for a research reactor is generally produced by metallothermic reduction of UF_4. The performance of metallothermic reaction and the recovery of uranium largely depend on the properties of UF_4. As ADU is the first powder product in the process flowsheet, properties of UF4 largely depend on the properties of ADU. In the present paper, ADU is produced via both routes. Variation of uranium recovery and composition of ADU, with change in time, has been studied. It was observed that initially pH increased slowly. Then there was a small reduction in pH followed by an almost flat zone, and then there was a sharp increase in pH followed by a slow increase in pH. The first precipitation point was detected by the appearance of turbidity, which was further found to coincide with the reduction of pH. ADU obtained at inception via the UNS route consisted of orthorhombic $3UO_3.NH_3.5H_2O$. Another hexagonal phase ($2UO_3.NH_3.3H_2O$) appeared in ADU with further addition of NH_3. It was further observed that pH of the solution increased continuously during ADU precipitation via the UFS route. However, precipitation started at a higher pH and uranium recovery was less compared with the production via the UNS route. It was further studied that the ADU produced at the inception via the UFS route consisted of $(NH_4)_3UO_2F_5$ (orthorhombic), and with further addition of ammonia, composition of ADU was changed and it became a mixture of $(NH_4)_3UO_2F_5$ (orthorhombic), $2UO_3.NH_3.3H_2O$ (hexagonal), and (NH_4) $(UO_2)_2F_5.4H_2O$ (hexagonal). The extent of $2UO_3.NH_3.3H_2O$ (hexagonal) increased with the progress of a reaction. Uranium recovery during ADU precipitation via the UNS route is more than that via the UFS route. The reduction of UO_3 to UO_2 is less in the UFS route than in the UNS route due to the presence of fluoride in ADU and subsequent UO_3. This causes an increase of UO_2F_2 content in UF_4 produced via the UFS route. The SSA of UO_2, obtained from the UFS route is less than that from the UNS route. This is why the UF_4 produced via the UFS route contained more unconverted uranium oxide than the UF_4 produced via the UNS route. Crystal-phase analysis shows that, in spite of the different compositions of the ADU produced by the two routes, the crystal structures of UO_2 and UF_4 produced by two different routes were similar.

Conflicts of interest

The authors have no conflicts of interest to declare.

Acknowledgments

The authors acknowledge Shri U.R. Thakkar, Smt. S. Thakur, and Shri K.N. Hareendran of UED, BARC, for their kind guidance and support to carry out the study.

REFERENCES

[1] International Atomic Energy Agency, Specific Considerations and Milestones for a Research Reactor Project, IAEA-NP-T-5.1, IAEA, Vienna, 2012.
[2] International Atomic Energy Agency, Strategic Planning for Research Reactors, IAEA-TECDOC-1212, IAEA, Vienna, 2001.
[3] International Atomic Energy Agency, Applications of Research Reactors, IAEA-NP-T-5.3, IAEA, Vienna, 2014.
[4] International Atomic Energy Agency, Commercial Products and Services of Research Reactors, IAEA-TECDOC-1715, IAEA, Vienna, 2013.
[5] A.M. Saliba-Silvat, E.F. Urano de Cai Valhot, H.G. Riella, M. Durazzo. Research reactor fuel fabrication to produce radioisotopes [Internet]. In: N. Singh (Ed.), Radioisotopes—Applications in Physical Sciences, InTech. Available from: http://www.intechopen.com/books/radioisotopes-applications-in-physical-sciences/research-reactor-fuel-fabrication-to-produce-radioisotopes (Accessed 15 July 2016).
[6] International Atomic Energy Agency, The Applications of Research Reactors, IAEA-TECDOC-1234, IAEA, Vienna, 1999.
[7] C.D. Harrington, A.E. Euchle, Uranium Production Technology, D. Van Nostrand Company Inc., Princeton, 1959.
[8] C.K. Gupta, H. Singh, Uranium Resource Processing: Secondary Resources, Springer, New York, 2003.
[9] S. Manna, U.R. Thakkar, S.K. Satpati, S.B. Roy, J.B. Joshi, J.K. Chakravartty, Study of crystal growth and effect of temperature and mixing on properties of sodium diuranate, Prog. Nucl. Energy 91 (2016) 132–139.
[10] S. Manna, C.B. Basak, U.R. Thakkar, S. Thakur, S.B. Roy, J.B. Joshi, Study on effect of process parameters and mixing on morphology of ammonium diuranate, Radioanal. Nucl. Chem. 310 (2016) 287–299.
[11] W.T. Bourns, L.C. Watson, Preparation of Uranium Dioxide for Use in Ceramic Fuels—Part I: Batch Precipitation of Ammonium Diuranate, Report, Atomic Energy Canada Limited, 1958.
[12] A.M. Deane, The infra-red spectra and structures of some hydrated uranium trioxides and ammonium diuranate,, J. Inorg. Nucl. Chem. 21 (1961) 238–252.
[13] A. Deptula, A study of composition of ammonium uranates,, Nukleonika 7 (1962) 265–275.

[14] E.V. Garner, X-ray diffraction studies on compounds related to uranium trioxide dehydrate, J. Inorg. Nucl. Chem. 21 (1962) 380–381.
[15] E.H.P. Cordfunke, On the uranates of ammonium-I: the ternary system NH_3-UO_3-H_2O, J. Inorg. Nucl. Chem. 24 (1962) 303–307.
[16] P.C. Debets, B.O. Loopstra, On the uranates of ammonium-II: X-ray investigation of the compounds in the system NH_3-UO_2-H_2O, J. Inorg. Nucl. Chem. 25 (1963) 945–953.
[17] M.E.A. Hermans, T. Markestein, Ammonium urinates and UO_3-hydrates ammoniates, J. Inorg. Nucl. Chem. 25 (1963) 461–462.
[18] S.D.L. Roux, A. Van Tets, The space group determination from a single crystal of a member of the ADU family on a reciprocal lattice explorer, J. Nucl. Mater. 119 (1983) 110–115.
[19] S. Manna, S. Chowdhury, S.K. Satpati, S.B. Roy, Prediction of firing time of magnesio thermic reduction (MTR) reaction and study of relative importance of the dependent parameters using artificial neural network, Indian Chem. Eng. 49 (2007) 221–232.
[20] S.V. Mayekar, H. Singh, A.M. Meghal, K.S. Koppiker, Magnesio-thermic reduction of UF4 to uranium metal: plant operating experience, Proceedings of National Symposium on Uranium Technology, BARC, Trombay, 13–15 December, 1989.
[21] N.P. Galkin, Technology of Uranium, Israel Program for Scientific Translations Ltd, Jerusalem, 1966.
[22] B. Tomazic, M. Samarzija, M. Branica, Precipitation and hydrolysis of uranium (VI) in aqueous solutions—VI: investigation on the precipitation of ammonium uranates, J. Inorg. Nucl. Chem. 31 (1969) 1771–1782.
[23] N.Q. Dao, On the formation of alkali uranates in aqueous solutions. A general review, Bull. Soc. Chim. Fr. 6 (1968) 2043–2047.
[24] V.P. Seleznev, A.A. Tsvetkov, B.N. Sudarikov, B.V. Gromov, Investigation into uranyl fluoride hydrates, Russ. J. Inorg. Chem. (Engl. Transl.) 16 (1971) 1174.
[25] J.L. Woolfrey, The preparation of UO_2 powder: effect of ammonium uranate properties, J. Nucl. Mater. 74 (1978) 123–131.
[26] G.H. Price, Self reduction in ammonium urinates, J. Inorg. Nucl. Chem. 33 (1971) 4085–4092.
[27] Calculated from ICSD (Inorganic Crystal Stucture Database) Using POWD-12++ 85, 1997, p. 135.
[28] P. Taylor, D. Wood, A. Duclos, The early stages of U_3O_8, formation on unirradiated CANDU UO_2 fuel oxidized in air at 200–300°C, J. Nucl. Mater. 189 (1992) 116–123.
[29] D. Smith, ICDD Grant-in-Aid, Penn State University, University Park, Pennsylvania, USA, 1979.
[30] Calculated from ICSD (Inorganic Crystal Stucture Database) Using POWD-12++ 39, 1997, p. 75.
[31] R. Fritsche, C. Sussieck-Fornefeld, ICDD Grant-in-Aid, Min.-Petr. Inst., Univ., Heidelberg, Germany, 1988.
[32] Calculated from ICSD (Inorganic Crystal Stucture Database) Using POWD-12++ 101, 1997, p. 9333.